Centrifugal Liquid-Liquid Separation - Experimental Investigation and Simulation of Single Drops and Droplet Swarms

Armin EGGERT[1,*], Stephan SIBIRTSEV[1] and Andreas JUPKE[1]

[1] *AVT - Fluid Process Engineering, RWTH Aachen University, Forckenbeckstraße 51, 52074 Aachen, Germany,*

Fundamentals of the liquid-liquid separation behavior, sedimentation and coalescence, under enhanced force field – the centrifugal field – are investigated experimentally and simulated by detail models. The single drop sedimentation shows an angular deflection against the radial trajectory. Further, a decrease of the sedimentation velocity due to the radial deceleration within the centrifugal force field is determined. The single drop sedimentation, the influences of droplet diameter and rotation speed are presented by radius-angle coordinates and by radius/angle-time coordinates. In addition the liquid-liquid separation with an increased organic droplet hold-up is presented. Compared to the single drop sedimentation a significant lower sedimentation velocity of the droplet swarm is observed. Finally the influence of the droplet swarm on the sedimentation velocity is discussed. Thus, to take the geometric feature of the cylindrical equipment into account of the swarm impact a correlation is developed by a modification of the droplet swarm model.

1. Introduction

Gravity separation of liquid-liquid mixtures - e.g., in settling tanks – is well investigated. Major phenomena of the separation behavior, e.g., the flow pattern, are understood in detail. Thus, sedimentation as well as coalescence effects of single drops and droplet swarms are combined for reliable settler design by a nowadays established experimental lab-scale/model-based approach [1]. However, for centrifugal liquid-liquid separation - e.g., in tube centrifuges, shown by the colored rotor zone of the Annular Centrifugal Contactors (ACC) in Figure 1 - only a few detailed investigations are given in available literature.

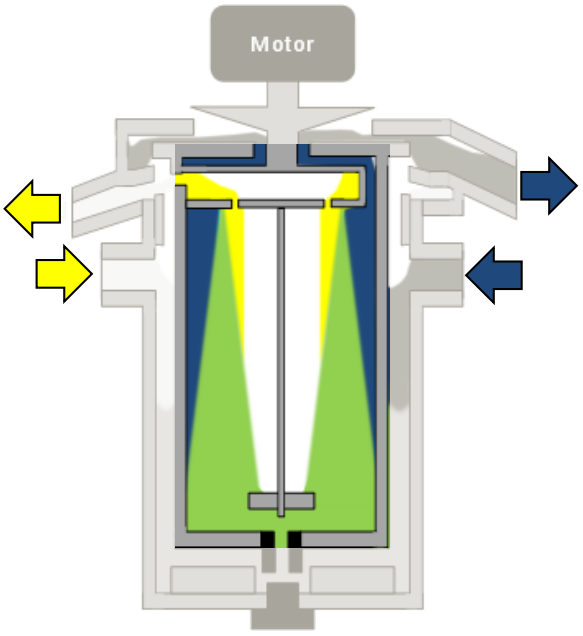

Figure 1. Schematic of an Annular Centrifugal Contactor (ACC), inflow and outflow of the heavy phase (blue), the light phase (yellow) and the centrifugal separation of their mixture (green) within in the rotor-zone.

Despite that an optical validation of the liquid-liquid separation within the rotor of an ACC is not possible Computer Fluid Dynamic (CFD) simulations are investigated by different authors [2–5]. Further a first approach for the determination of the single fluid flow pattern with the particle image velocimetry (PIV) method could be found [6]. An empiric correlation, developed by black box investigation of separation efficiency is given in the general form by Equation (1) [7]. N_{Di} is called the "Dispersion Number" and proposed a relation between the acceleration of a disperse system and the overall separation time t for a fixed geometric $\Delta Z = r_o - r_i$, meaning the outer and inner diameter of the rotor zone.

$$N_{Di} = \frac{1}{t} \cdot \sqrt{\frac{\Delta Z}{a}} = \frac{1}{t} \cdot \sqrt{\frac{r_o - r_i}{a}} \quad (1)$$

More detailed investigation of the drop motion, preferably the motion of droplet collectives and their coalescence behavior within the centrifugal force field is carried out for the Podbielniak differential centrifugal extractor [8–10]. Also, the sedimentation is discussed for monodispersed drop strings [11]. However, a broad knowledge gap exists in the detailed understanding and research of centrifugal continuously liquid-liquid separation in the rotor zone of an ACC. Thus, this contribution focuses on the major liquid-liquid separation effects and their quantification within a centrifugal force field. The single drop sedimentation and the liquid-liquid separation will be characterized by sedimentation, coalescence and the overall separation time as done for the gravitational settling tank. Furthermore, the individual models will be combined for a model-based centrifugal equipment design.

2. Experimental

2.1 Chemical system

For experimental investigations n-butanol/water and toluol/water were chosen as liquid-liquid systems. Their physical properties are summarized in Table 1. N-butanol was provided by Merck, Darmstadt, Germany, with a purity of 99 %. Toluol was provided by CarlRoth, München, Germany, with a purity of 98 %. The aqueous phase was deionized and distillated in a MonoDest3000 distillery from Lenz Glas Instrumente, Wertheim, Germany. Furthermore sodium chloride (NaCl), provided by Merck, Germany, with purity of 99 %, was used for water conditioning – 5 g_{NaCl}/kg_{H2O}.

Table 1. Physical properties of saturated liquid-liquid systems

System		ρ [kg/m³]	η [mPas]	σ [mN/m]	phase state
1	water	987	1,463	1,75	continuous
	n-butanol	846	3,32		dispersed
2	water	999	1,323	3,8	continuous
	toluol	867	2,31		Dispersed

2.2 Experimental setup

Experiments for single drop sedimentation and liquid-liquid separation behavior of droplet

swarms within the centrifugal field are performed with two different experimental set-ups at laboratory scale, as shown in Figure 2. The set-up on the left side (A) enables a single drop induction by a capillary system. The set-up on the right side (B), the stirred centrifugal batch settling cell (SCBSC) [12], enables the mixing and the separation of a liquid-liquid system by a rotor-rotor/stator concept. Both, the centrifugal cell body and the agitator are driven by separate electric motors. Thus, the elements can run synchronously or with a differential rotational speed, $\Delta n = n_C - n_A$. For chemical resistance all components of the SCBSC are made out of stainless steel (1.4401), polypropylene (PP), polytetrafluorethylene (PTFE) and glass.

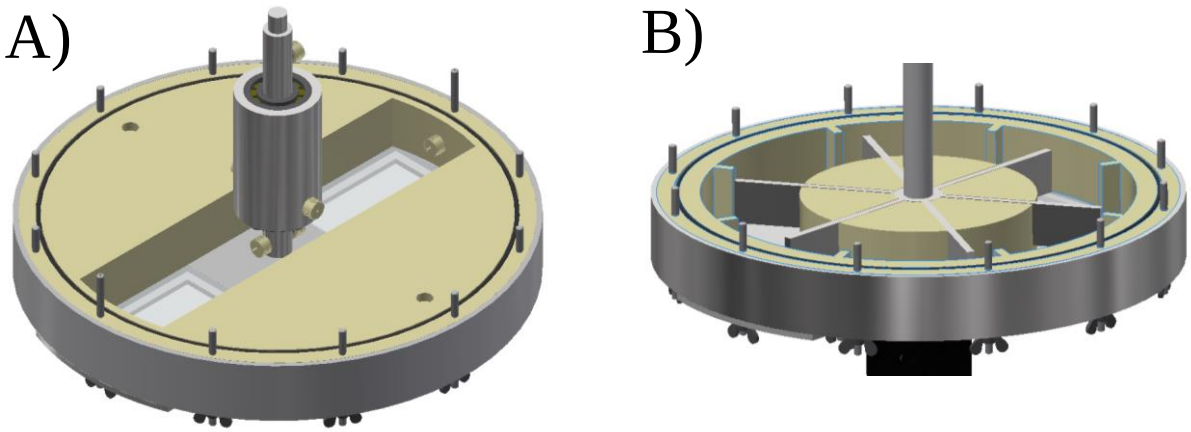

Figure 2. Experimental set-up for A) single drop sedimentation and B) liquid-liquid separation – the SCBSC – investigation within the centrifugal field.

For the optical observation a high speed video camera (type: Os4S1-C-O4, 8 GB DDR working storage, 512 GB SSD intern storage, 1024x1024 pixels, 6.000 frames per second (fps), supplied by Imaging Solutions GmbH, Eningen, Germany) with a camera objective (type: LM16HC, 1'' 16mm/F1.4, supplied by Kowa Optimed Deutschland GmbH, Duesseldorf, Germany) is used. The camera focused on the centrifugal cell front surface with integrated glass windows. The camera is triggered by a laser light barrier and a trigger marker on the cylinder wall. Camera and recording settings are controlled via Ethernet linkage and the Motion Studio PC software (v. 2.12.05). For a sufficient lighting performance, required for short exposure times, a 500 W light emitting diode (LED) is used. The 500 W LED is powered by a direct current (DC) laboratory power supply (type: PS 8360-10 T, 0…360 V, 0…10 A, up to 1,000 W, supplied by Elektro-Automatik GmbH & Co. KG, Viersen, Germany).

2.3 Analytical method

The analytical method is based on the optical observation of the droplet sedimentation and the liquid-liquid separation during the centrifugation process. The sedimentation and separation progress is quantified by path-time coordinates following a radial trajectory to the axis of rotation. Each path coordinate includes a value for the sedimentation (radial, azimuthal) and coalescence progress. In this way, the characteristic separation curves, sedimentation and coalescence, are determined.

3. Simulation

3.1 Model

The theoretical part of this work focuses on the implementation of a single drop motion model for the calculation of the single drop sedimentation velocity v_∞ and further the combination with a droplet swarm correlation for the calculation of the droplet swarm sedimentation velocity v_{DS}.

The particle motion model in the most general form is given in Equation (2) [13], where ρ is the density of the disperse or continuous phase, W the velocity of the droplet, ω the angular frequency, r the radius, V the droplet volume and η the viscosity. In contrast to the gravitational force field the unsteady acceleration is considered by the added mass and Basset history term. From literature work the including constants are set to $\Delta_A = 2.0$ and $\Delta_H = 0.48$ [14]. Especially the estimation and the use of a valid drag force coefficient c_D correlation, as given in Equation (3) [15] as a function of the droplet Reynolds number, was a necessary work before the swarm influence could be focused on.

$\rho_d V_d \frac{dW}{dt} = V_d(\rho_d - \rho_c)\omega^2 r - \frac{1}{2} V_d \rho_c c_D W^2 - \Delta_A \frac{1}{2} V_d \rho_c \frac{dW}{dt}$	
$-\frac{3}{2}\Delta_H {d_d}^2 \sqrt{\pi \rho_c \eta_c} \int_0^t \left(\frac{\left(\frac{dW}{dt}\right)_{t=\tau_1}}{\sqrt{t-\tau_1}} \right) d\tau_1$	(2)
$c_{D,\infty} = 239 / {Re_\infty}^{0.956}$	(3)

For the calculation of the droplet swarm sedimentation velocity the definition of the Reynolds Droplet Swarm Re_{DS} as given in Equation (4) and the empirical model proposed as given in Equation (5) [16] with the organic hold-up ε and the Hadamard-Rybczynski-correction factor are used. For the prediction of the droplet swarm drag coefficient c_{D_DS} Equation (6) is applied.

$$Re_{DS} = \rho_c v_{DS} \Phi_{32,0} / \eta_c \tag{4}$$

$$Re_{DS} = 3zq^2\varepsilon_0 / c_w' q^3 (1-\varepsilon_0) \left(\sqrt{1 + c_w' q^3 (1-\varepsilon_0)^3 / 54 (zq^2)^2 {\varepsilon_0}^2 \, Ar} - 1 \right) \text{ with:} \tag{5}$$

$$q^3 = 5 \left(\varepsilon_0 / 1-\varepsilon_0 \right)^{0,45} K_{HR}^{-3/2}$$

$$zq^2 = \frac{1-\varepsilon_0}{2\varepsilon_0 K_{HR}} \exp\left(2.5\varepsilon_0 / 1-0.61\varepsilon_0 \right) \quad \text{for } 0.06 \le \varepsilon_0 < 0.55$$

$$zq^2 = 2.2 \frac{1-\varepsilon_0}{2\varepsilon_0 K_{HR}} \exp\left(0.44\varepsilon_0 / 1-0.61\varepsilon_0 \right) \quad \text{for } 0.55 \le \varepsilon_0 < 0,74$$

$$c_{D\_DS} = c_{D,\infty}(1-\varepsilon_0)^{-2n} \quad \varepsilon(r_{DS})/\varepsilon_0 \tag{6}$$

Finally, the increase of the initial droplet hold-up is modified and takes into account the geometric influence / radial impact by the correlation as shown in Equation (7).

$$\varepsilon(r_{DS}) = \varepsilon_0 \quad r_0/r_{DS} \tag{7}$$

4. Results and Discussion

4.1 Single drop sedimentation

Figure 3 shows an experimental result of the single drop sedimentation for the toluol/water-system. For illustration and better understanding of the presented radius(y)-angle(x) coordinate pairs an image from the experimental work is given in the figure where drops are marked with withe cycles. The rotational speed is set to n = 1100 rpm. Depending on the used nozzle the centrifugal force leads to a drop diameter of d_T = 0.8 mm. Also the model-based calculated drop trajectory is plotted in the figure. Both, the experiment and the simulation are in good agreement. Moreover, the single drop motion model matches the experimental data quite well. The radius-angle relation shows the Coriolis Effect. Hence, the single drop motion is affected by the drop diameter, the liquid-liquid system properties, especially the density difference and continuous phase viscosity, and centrifugal operating parameters.

The sedimentation progress in radius(y)-time(x) coordinates is shown in Figure 4. It is anticipated that the sedimentation describes a nonlinear sedimentation pathway over the time. This could be observed by a decrease of the radial distance between the drops. This effect is explainable by the centrifugal acceleration based unsteady sedimentation velocity. Thus, the negative gradient of the centrifugal field which leads to a deceleration, affected the drop motion.

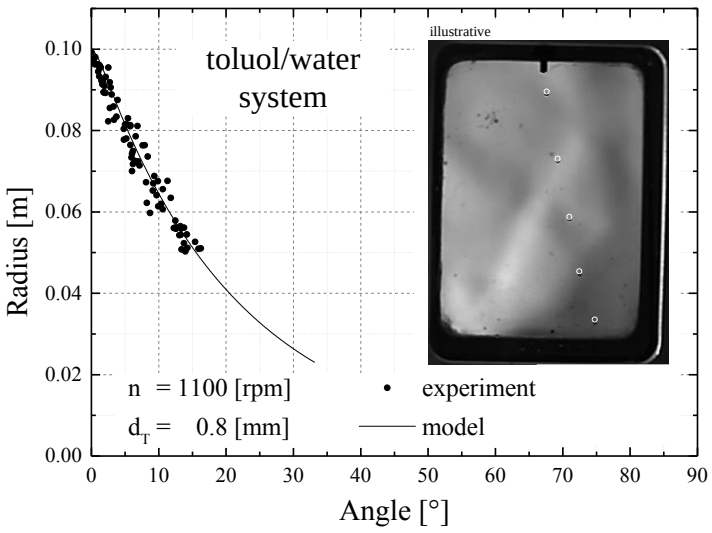

Figure 3.
Single drop investigation - result for droplet (d_T = 0.8 mm) sedimentation at n = 1100 rpm. The diagram shows an experimental evaluation of the droplet trajectory (●) and the simulated drop motion (·····) by radius-angle coordinates. The image shows the experimental evaluation with marked drops.

4.2 Liquid-liquid separation

Figure 4 shows an experimental result of the liquid-liquid separation of the n-butanol/water-system. The differential rotational speed for mixing is set to $\Delta n = 500$ rpm and the rotational speed for separation is set to $n = 1100$ rpm. The phase ratio is $V_{org}:V_{aq} = 1:1$ and thus, the start hold-up is $\varepsilon_0 = 0.5$. For the illustration and better understanding of the experimental result images from different separation times are given in the Figure. Depending on the centrifugal field the organic disperse phase flows from the outer to the inner radius. Opposite the coalescence occurs from inner to outer radius. In the pictures the dispersion band and thus the sedimentation as well as the coalescence front can be identified clearly. Furthermore, the shadow in the bottom shows the displacer of the CSBSC which enables the mixing process without a gas hold-up in the entire volume. Compared to the single drop sedimentation the sedimentation curve describes a nonlinear path way. While sedimentation starts instantaneous the coalescence starts delayed. This phenomenon is explainable by the linear increase of the location-depended centrifugal acceleration. Subsequently, the initial drop hold-up increases along the radial trajectory before coalescence takes place. Thus, the geometric impact needs to be considered in the model approach.

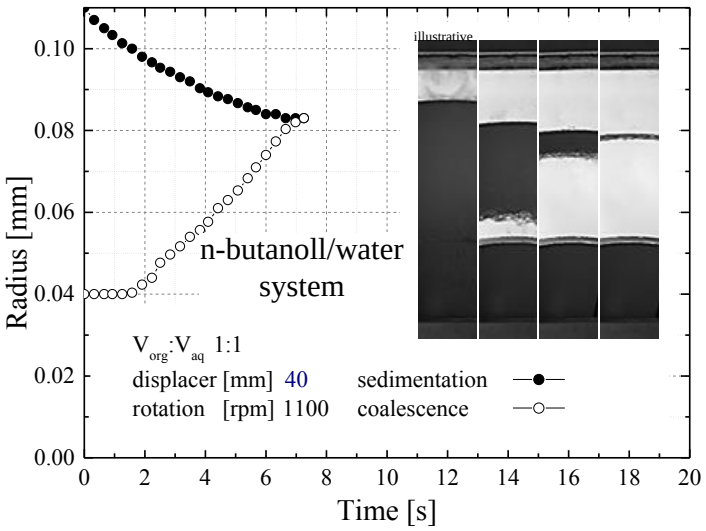

Figure 4. Liquid-liquid separation - droplet swarm sedimentation and coalescence. The picture show an experimental result for the separation progress ($\varepsilon_0 = 0.5$) at $n = 1100$ rpm and the diagram shows an experimental evaluation of the sedimentation (●) and coalescence (○) by radius-time coordinates.

4.3 Swarm impact

Figure 3 shows a simulation result for the single drop and droplet swarm sedimentation behavior. The rotational speed is set to $n = 1100$ rpm and the hold-up is set to $\varepsilon_0 = 0.5$. The drop diameter is $d_d = 0.6$ mm. Based on the simulation results the impact of the drop hold-up is shown qualitatively. The change in radial position is plotted in black lines and the calculated sedimentation velocity in red lines. The single drop results are visualized by the solid lines, the droplet swarm with a constant hold-up by dashed lines and the influence of the geometric impact with an increasing radial hold-up by dotted lines. The droplet swarm influences the free sedimentation by a higher droplet hold-up. Thus, in the shown figure the sedimentation velocity decreases significantly compared to the single drop trajectory. Depending on the slower sedimentation velocity the radial position of the sedimentation

front decreases slower. This results in an increase of the overall sedimentation time. Further, another difference is visualized by the hold-up correction. In the beginning, the initial hold-up and thus the sedimentation velocity are the same, then the theoretical increase of the circumference related hold-up leads to a distinct swarm impact. However, the sedimentation limit depends on the abstraction and model description. As shown in Figure 3 the phase boundary level for the liquid-liquid separation of an entire hold-up of $\varepsilon_0 = 0.5$ and the displacer is up to $r_E > 0.08$ m.

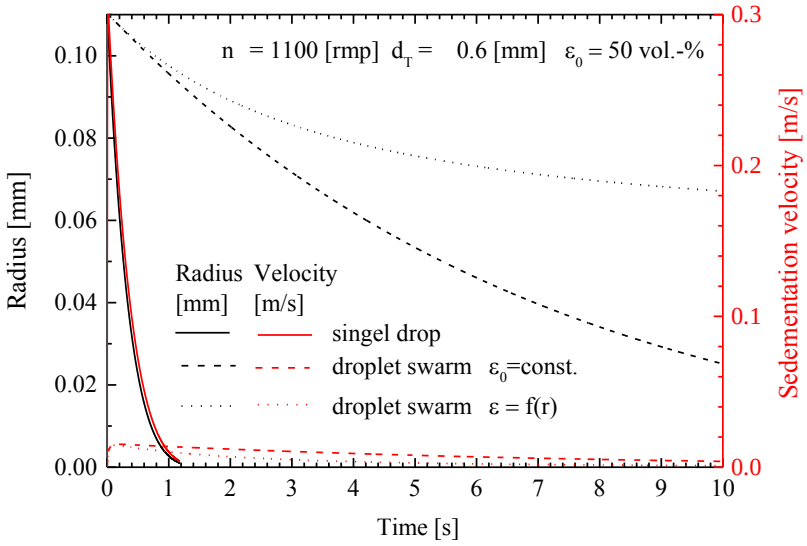

Figure 5.
Simulation results for the radial sedimentation (black) and the sedimentation velocity (red) for a single drop (——) and a droplet swarm with constant hold-up (- - -) and increasing hold-up (· · ·). The rotational speed is n = 1100 rpm, the droplet diameter is $d_T = 0.6$ mm and the start hold-up is $\varepsilon = 0.5$.

5. Conclusion

Centrifugal singel drop sedimentation and liquid-liquid separation investigations were demonstrated sucsessfully. The liquid-liquid separation experiments are characterized by sedimentation, coalescence and the overall separation time. Model approches from gravitational investigations are sucessful implemented and combined for the centrifugal field. A modification of the droplet swarm model considered thecylindric geometirc impact. Thus, a significant decrease of the sedimentation velocity of the droplet swarm in comparison to singel drops is shown.

Acknowledgement

This work was performed as part of the Cluster of Excellence “Tailor-Made Fuels from Biomass”, which is funded by the Excellence Initiative by the German federal and state governments to promote science and research at German universities. Further, the authors thank RWTH Aachen University – department 4.1 Technology Transfer for the assumption of the patent application.

References

1) M. Henschke, *Fort. Berichte VDI*, **379**, (1994).
2) S. Li, W. Duan, J. Chen, J. Wang, *Ind. Eng. Chem. Res.,* **51**, 11245–11253, (2012).
3) N.T. Padial-Collins, D.Z. Zhang, Q. Zou, X. Ma, W.B. VanderHeyden, *Separation Science and Technology*, **41**, 1001–1023 (2006) 1001–1023.
4) J. Patra, N.K. Pandey, U.K. Muduli, R. Natarajan, J.B. Joshi, *Chem. Eng. Commu.*, **200**, 471–493, (2013).
5) S. Vedantam, K.E. Wardle, T.V. Tamhane, V.V. Ranade, J.B. Joshi, *Int. Journal of Chemical Engineering*, **94**, 1-31, (2012).
6) Y. Xu, J.-g. Wang, S.-l. Zhao, Z.-s. Bai, *Chem. Eng. Res. Des.*, **94**, 691-701 (2015).
7) R.A. Leonard, G.J. Bernstein, R.H. Pelto, A.A. Ziegler, *AIChE J.*, **27**, 495-503, (1981).
8) F. Otillinger, *Technical Universität Munich*, (1988).
9) M. Stölting, *Technical Universität Munich*, (1979).
10) R. Schilp, *Technical Universität Munich*, (1979).
11) Y. Jammoal, J. Lee, *Chemical Engineering Research and Design*, **104**, 638-646, (2015).
12) A. Eggert, *German Patent and Trademark Office*, (2016).
13) M.R. Maxey, J.J. Riley, *Physics of Fluids* **26**, 883-889 (1983).
14) D.J. Vojir, E.E. Michaelides, *Int. Journal of Multiphase Flow*, **20**, 547-556, (1994)
15) T. Fukada, S. Takeuchi, T. Kajishima, *Int. Journal of Multiphase Flow*, **85**, 298-313 (2016)
16) T. Pilhofer, D. Mewes, *Verlag Chemie*, (1979).